Low-dose CT Statistical Iterative Reconstruction Using Hyperbolic Tangent Enhanced Total Variation Regularization

Ming Li, Jingxin Liu, Cheng Zhang, Chengtao Peng, and Jian Zheng

Abstract—Nowadays, X-ray computed tomography (CT) has been widely used in the early detection and accurate diagnosis of various diseases. However, the inherent side effect of CT radiation, relating to cancer and other diseases, has caused great concerns in radiology. So how to reduce radiation dose immensely while maintaining image quality is a major challenge in CT imaging field. As a practical application of compressed sensing theory, the sparse constraint term referred to total variation (TV) minimization has already produced promising images for low dose CT reconstruction. However, the piecewise constant assumption of TV model often produces blocky artifacts in reconstructed images. To eliminate this drawback, we apply a family of hyperbolic tangent functions to enhance the sparse representation of TV model. Furthermore, a dynamic regularization term is also introduced to improve the performance of the proposed model. In our method, the proposed constraint term is incorporated into an objective function in a statistical iterative reconstruction (SIR) framework. We evaluate the proposed method using X-ray projections collected from simulated phantoms and scanned mice. And the results show that the presented approach can produce better images when compared to several existing methods in terms of lower noise and more anatomical features.

I. INTRODUCTION

NOWADAYS, X-ray computed tomography is undoubtedly an effective and reliable tool and widely used in hospitals for diagnosis and intervention. However, the overdose of X-ray radiation possibly increases the risk of cancer and other genetic diseases. Therefore, the radiation risk issue has attracted more and more research attention. Using the low-dose scan protocols can be the most straightforward and pragmatic solution [1]. Since X-ray imaging is a quantum accumulation process, the signal-to-noise ratio (SNR) depends on the X-ray dose quadratically. Hence, given the noisy measurements, the

images reconstructed via conventional analytical reconstruction methods will suffer from increasing noise and artifacts. Another approach is to produce insufficient projection data, which will lead to limited-angle, few-view, interior scan, or other problems [2, 3].

To reconstruct images from noisy and insufficient measurements, various image reconstruction approaches have been extensively investigated. Among them, statistical iterative reconstruction (SIR) methods for X-ray CT use realistic models that incorporate the statistical properties of the noise and the imaging geometry of the data acquisition [4-7]. Compared to the conventional filtered back-projection (FBP) reconstructions, SIR methods provide improved spatial resolution and noise properties, along with other potential advantages such as reduced patient dose and artifacts. Usually, the cost functions of the SIR methods contain two components, i.e., the data-fidelity term and regularization term. The data-fidelity term models the statistical properties of the noise and is prerequisite for the success of the SIR methods in clinical applications. The regularization term reflects the prior information of the reconstructed image aiming to regularize the solution. Recently, compressive sensing (CS) based regularization designs have become popular, and have been widely used for X-ray CT reconstruction from incomplete and noisy datasets. A typical example is TV regularization via the discrete gradient transform (DGT). Extensive studies have shown that high-quality CT image can be reconstructed via TV minimization from insufficient and noisy acquisitions without producing obvious artifacts [8]. However, the DGT operation cannot distinguish between true structures and image noise. Consequently, the image reconstructed via TV regularization may lose detailed features and lead to noticeable patchy artifacts. Hence, it is imperative to investigate superior sparsifying methods for CS-inspired image reconstruction.

It is well-known that the l_0 norm regularization can provide a sparser representation than the TV regularization (l_1 norm). However, the application of l_0 norm in image reconstruction is often a non-deterministic polynomial-time (NP) hard problem due to the fact that the l_0 norm is a non-convex function in discontinuous form. Therefore, several alternatives have been proposed to obviate this drawback. The first idea of reweighted TV (RWTV) originates from the effort of minimizing a concave function that approximates the l_0-norm, which can eventually be converted to solve a sequence of reweighted

l_1-norm problems [9]. The RWTV approach can be easily solved, but may lead to over-smoothing edge details. Other approximate options including tunable fractional order norm, are simply expressed, but may lead to complicated parameters estimation [10, 11]. Recently, a sparse representation method via smoothed l_0 (SL0) approximation has attracted an increasing interest in the signal processing fields. In order to deal with the discontinuities in the l_0 norm, a family of continuous functions can be summed up to approximate the l_0 norm [12]. In this study, we use a family of hyperbolic tangent functions to enhance the sparse representation of TV model. Furthermore, a flexible modulation parameter is also introduced to implement dynamic regularization constraint.

In this work, we propose a hyperbolic tangent enhanced total variation (HTETV) model and incorporate it into an objective function in the SIR framework to address the low-dose CT reconstruction problem. The rest of this paper is organized as follows. We firstly review SIR algorithm and then detail the proposed HTETV regularization, the associative optimization algorithm, and the parameters setting. After that, a series of experiments are performed and corresponding discussions are given. Finally, there is a brief conclusion at the end of this paper.

II. METHODS

A. Statistical iterative reconstruction

According to previous work [4], the SIR problem is equivalent to the following minimization.

$$\Psi(x) = \sum_{i=1}^{I} \frac{w_i}{2} ([\mathbf{A}x]_i - l_i)^2 + \beta R(x) \tag{1}$$

Where $\mathbf{A} = \{a_{ij}\} \in \mathbb{R}^{I \times N^2}$ is the system matrix; $\mathbf{x} = (x_1, x_2, ..., x_{N \times N})^T$ is a linear attenuation coefficient distribution, which transforms the initial image of $N \times N$ pixels to a vector $\mathbf{x} \in \mathbb{R}^{N^2 \times 1}$; $\hat{l} = (\hat{l}_1, \hat{l}_2, ..., \hat{l}_I)^T$ is the measured data of l calculated by $\hat{l}_i = \ln(b_i / (y_i - r_i))$, while $l = (l_1, l_2, ..., l_I)^T$ is the integral of the linear attenuation coefficients with $l_i = [\mathbf{A}\mathbf{\mu}]_i = \sum_{j=1}^{N^2} a_{ij}\mu_j$, r_i accounts for the mean number of background events and read-out noise variance, $\mathbf{y} = (y_1, y_2, ..., y_I)^T$ is the scanning data, $\mathbf{b} = (b_1, b_2, ..., b_I)^T$ is the air exposure data; $w_i = (y_i - r_i)^2 / y_i$ is the statistical weight; β is a regularization parameter to balance the log-likelihood and penalty terms.

B. The proposed HTETV regularization

According to the CS-based reconstruction theory, the l_0-norm is simply expressed the number of nonzero components in x, and is given by,

$$\|x\|_0 = \lim_{\varsigma \to 0} \left\{ |x_1|^\varsigma + \cdots + |x_{N_j}|^\varsigma \right\}. \tag{2}$$

Despite Eq. (2) offers the highest possibility of sparse recovery with few measurements, some problems still exist in searching for a solution with minimal l_0 norm. It is usually stated in the literature that searching the minimum l_0 norm is NP-hard, and it is too sensitive to noise (because any small amount of noise can change the number of zero components significantly). The problems of using l_0 norm (that is, NP-hard and too sensitive to noise) are both due to the fact that the l_0 norm of a vector is a discontinuous function. In order to deal

with the discontinuities in $\|x\|_0$. Our idea is to approximate this discontinuous function via a suitable continuous one, and minimize it by means of a minimization algorithm for continuous functions (e.g. steepest decent method). Furthermore, a flexible modulation parameter (say σ) is also introduced to determine the approximation degree. In this study, the family of hyperbolic tangent functions is considered and can be expressed as

$$f_\sigma(x) = \frac{\exp(|x|/\sigma) - \exp(-|x|/\sigma)}{\exp(|x|/\sigma) + \exp(-|x|/\sigma)}, \tag{3}$$

and the corresponding SL0 approximation is

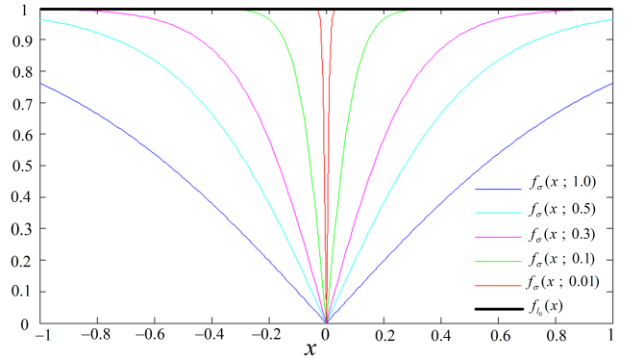$$F_\sigma(x) = \sum_{j=1}^{N^2} f_\sigma(x_j). \tag{4}$$

Fig. 1. Comparison of the proposed regularization functions and the l_0 regularization function.

It is clear from Fig.1 that $\|x\|_0 \approx F_\sigma(x)$, for small values of σ, and the approximation tends to equality when $\sigma \to 0$. Consequently, we can find the minimum l_0-norm solution via minimizing the substituted function $F_\sigma(x)$.

In the 2D image space, the image TV model can be defined as

$$TV(x) = \|Dx\|_1, \tag{5}$$

where $D_j x = D_{m,n} x = \sqrt{(x_{m,n} - x_{m+1,n})^2 + (x_{m,n} - x_{m,n+1})^2}$. If we apply Eq. (4) to enhance the sparse representation of TV model, then the composite function model of the linear attenuation coefficients x can be built. And the proposed HTETV regularization can be expressed as

$$R(x) = F_\sigma(TV(x))$$
$$= \sum_{j=1}^{N^2} \left\{ \frac{\exp(\|D_j x\|_1 / \sigma) - \exp(-\|D_j x\|_1 / \sigma)}{\exp(\|D_j x\|_1 / \sigma) + \exp(-\|D_j x\|_1 / \sigma)} \right\}, \tag{6}$$

where σ is a dynamic regularization parameter used to determine the smoothness of the function $R(x)$. The larger value of σ produces the smoother $R(x)$, which will result in worse approximation to l_0 norm; the smaller value of σ offers the better behavior of $R(x)$ close to l_0 norm, but speckle noises may appear in the final reconstructions.

C. Optimization algorithm

There are two key components for the optimization scheme of the proposed cost function. The first component is the SIR process that enforces the statistical knowledge. The second component is the HTETV based sparse representation. In this paper, we first use the separable paraboloid surrogate method to minimize the log-likelihood term

$$x_j^t = x_j^{t-1} - \frac{\sum_{i=1}^{N_d}\left(a_{i,j}\, y_i\left([\mathbf{A}x^{t-1}]_i - \hat{l}_i\right)\right)}{\sum_{i=1}^{N_d}\left(a_{i,j}\, y_i \sum_{k=1}^{J} a_{i,k}\right)}, \qquad j=1,...,J \tag{7}$$

where the superscript $t=1,2,...$ is the iteration number. In step two, the gradient descent method is used to minimize the proposed HTETV model. According to the derivation rule of the compound function, the derivative of HTETV is defined as

$$\frac{\partial R(x)}{\partial x_j} = \sum_{j=1}^{N_J}\left\{ \frac{4}{\left(\exp(\|D_j x\|_1/\sigma) + \exp(-\|D_j x\|_1/\sigma)\right)^2} \cdot \frac{1}{\sigma} \cdot \frac{\partial TV(x_j)}{\partial x_j} \right\}, \tag{8}$$

where the derivative of TV is

$$\frac{\partial TV(x_j)}{\partial x_j} = \frac{\partial TV(x_{m,n})}{\partial x_{m,n}} = \frac{2x_{m,n} - x_{m+1,n} - x_{m,n+1}}{\sqrt{(x_{m,n}-x_{m+1,n})^2 + (x_{m,n}-x_{m,n+1})^2 + \varepsilon}}$$
$$- \frac{x_{m-1,n} - x_{m,n}}{\sqrt{(x_{m-1,n}-x_{m,n})^2 + (x_{m-1,n}-x_{m-1,n+1})^2 + \varepsilon}} \tag{9}$$
$$- \frac{x_{m,n-1} - x_{m,n}}{\sqrt{(x_{m,n-1}-x_{m+1,n-1})^2 + (x_{m,n-1}-x_{m,n})^2 + \varepsilon}}$$

where ε is a small positive number (10^{-8} in our experiments), which prevents the derivative being singular in smooth regions. Therefore, our algorithm mainly consists of two steps: SIR iteration and HTETV minimization of the reconstructed image. However, the two steps play different roles in image reconstruction. SIR process can preserve more details in texture regions, but speckle noise will appear in the reconstructions. HTETV process can effectively suppress the blocky effect and also reduce the divergence of SIR, but the anatomical features can be easily obscured. Hence, when the two steps are repeated alternatively, the image quality will improve gradually.

D. Selection of σ

In the proposed HTETV model, the shape parameter σ determines the regularization function in Eq. (6), and plays a crucial role in improving reconstruction performance. If we select a teeny value of σ, the function $R(x)$ is highly unsmooth, and contains lots of local minimums, and hence its minimization is not easy. However, for larger values of σ, the function $R(x)$ becomes smoother and contains less local minimums, and its minimization is easier. At the initial iterations, the results of SIR own serious artifacts and noise, we use the more strong regularization effect via a larger value of σ to suppress artifacts and noise fully. Subsequently, we weaken the regularization effect gradually via orderly slightly decreasing values of σ, which is used to preserve more edge details in texture regions. Due to the fact that σ decreases gradually, for each value of σ, the minimization algorithm starts with an initial solution will get close to the actual minimum of $R(x)$. In this paper, we initially select $\sigma_0 = 0.9$, which offers a regularization model close to TV constraint. In order to guarantee the proximity of adjacent iterations, the decreasing factor ρ is selected within the range from 0.9 to 1.0. Meantime, the selection of σ should satisfy $\sigma_{\min} \geq 0.01$.

III. RESULTS AND DISCUSSIONS

A. Numerical phantom study

We first start our evaluation with the modified FORBILD head phantom dataset. The phantom is composed by 512×512 pixels with image array is 20cm×20cm. The projection data were generated according to the fan-beam CT geometry. The forward projection parameters were defined as: the source-to-axis distance was 54.1cm and the distance of axis-to-detector was 40.8cm. The projection data of each view included 642 bins and the size of each element was 0.672mm× 0.672mm. To demonstrate the performance of our method, three different datasets were produced with the views of 180, 240, and 360 during 2π rotation. After that, Poisson noise was added to each detector with the photon number 8×10^5. Fig. 2 shows the reconstructed results by different algorithms from the datasets acquired with the views of 180, 240, and 360, respectively. It can be observed that the images reconstructed via SIR-TV, RWTV, and SIR-HTETV algorithms are visually better than those by FBP in all cases. Furthermore, to make the otherness of the reconstructed results highlighted, the zoomed details of the ROI, as indicated by the red dotted rectangle in Fig. 2, within the results are shown in Fig. 3 to illustrate the improvement of the proposed SIR-HTETV algorithm. It can be seen that the present algorithm has better visual effect than other algorithms in the low contrast regions.
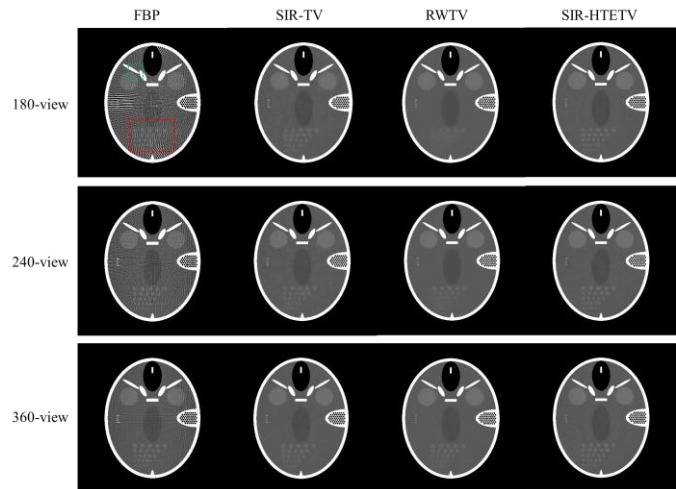

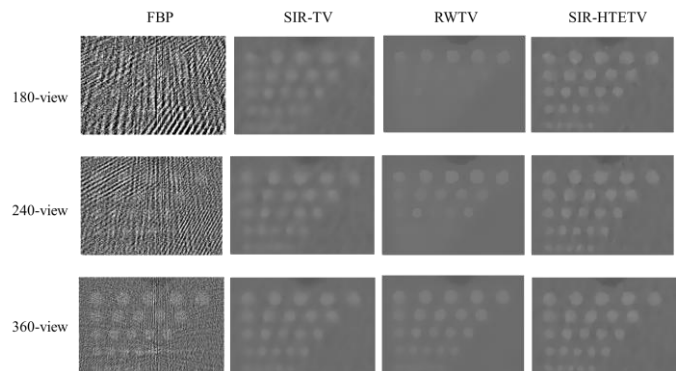Fig. 2. The results of modified FORBILD head phantom study.

Fig. 3. Zoomed details of the ROI in Fig. 2.

The following three metrics were used in this paper for quantitative analyses. To evaluate the noise suppression on the reconstructed images from low-dose measurement data, root normalized mean square error (RNMSE) and peak signal to noise ratio (PSNR) were selected in this study.

$$RNMSE = \left\{ \frac{\sum_{j=1}^{N_J}(x_j - x_j^{truth})^2}{\sum_{j=1}^{N_J}(x_j^{truth})^2} \right\}^{1/2} \qquad (10)$$

$$PSNR = 10\log_{10}\left(\frac{\max^2(x_j^{truth})}{\sum_{j=1}^{N_J}(x_j - x_j^{truth})^2 / (N_J - 1)} \right) \qquad (11)$$

To assess the performance of various algorithms at the local detail level, the structural similarity (SSIM) was used in this study.

$$SSIM(x, x^{truth}) = \frac{(2\bar{x} \cdot \bar{x}^{truth} + C_1)(2\sigma_{xx^{truth}} + C_2)}{(\bar{x}^2 + \bar{x}^{truth2} + C_1)(\sigma_x^2 + \sigma_{x^{truth}}^2 + C_2)} \qquad (12)$$

In order to evaluate the reconstruction results objectively, the PSNR, RNMSE, and SSIM were adopted to evaluate the reconstructed images. To calculate SSIM between the reconstructed results and the truth image, we selected the ROI, as indicated by the green dotted rectangle in Fig. 2. The corresponding quantitative results are shown in Table I. We can see that the proposed SIR-HTETV has the lowest RNMSE and the highest PSNR/SSIM for all cases.

TABLE I
COMPARING CRITERIONS OF THE RESULTS
RECONSTRUCTED BY DIFFERENT ALGORITHMS

	Views	FBP	SIR-TV	RWTV	SIR-HTETV
RNMSE	180	0.1908	0.0237	0.0207	0.0187
	240	0.161	0.023	0.0203	0.0182
	360	0.131	0.0211	0.0187	0.0181
PSNR	180	22.0901	40.1933	41.4	42.2853
	240	23.566	40.46	41.5649	42.4805
	360	25.3541	41.2014	42.248	42.5267
SSIM	180	0.9309	0.9931	0.997	0.9975
	240	0.9437	0.9945	0.9975	0.9987
	360	0.9585	0.9955	0.9983	0.999

B. Mouse data study

In this study, we evaluate the performance using actual datasets from the scanned mouse experiments in our lab. The X-ray tube voltage was set to be 50 kVp, the X-ray tube current was set to 1mA, and the exposure time was set to 0.4669s. The distance between the source and the center of rotation was 22.188cm, while the source-to-detector was 65.85cm. The number of bins per view was 1536×880, and the size of each bin was 0.15mm×0.15mm. To demonstrate the performance of our method, two different datasets were obtained with the projections of 180 and 360 during 2π rotation. From the cone-beam projection data, the central slice was extracted. The reconstructed image size was 512×512 with an isotropic pixel-size of 0.1mm×0.1mm. The reconstruction results are shown in Fig. 4. As can be seen, severe noise can be observed in the FBP results and the images appear to be blurry near to margin details. When compared with FBP, all three iteration methods work better in both suppressing noise and preserving tissue structures. Furthermore, the zoomed details of the ROIs, as indicated by the red circles in Fig. 4, and the zoomed images of this region are shown in the corresponding upper right corner. We can see that the proposed SIR-HTETV produces the best image quality with effective noise suppression and tissue structures preservation, especially the regions indicated by the red arrows.
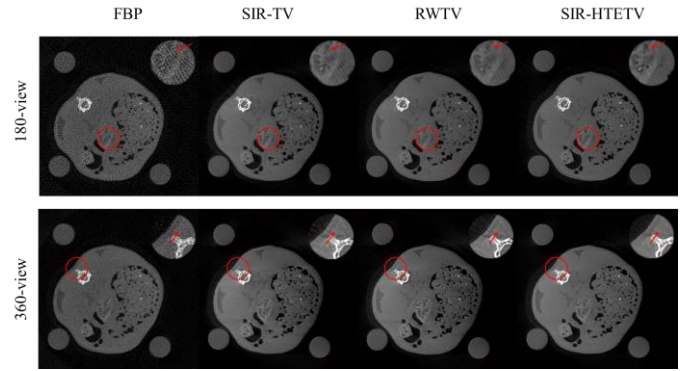

Fig. 4. The results of scanned mouse datasets.

IV. CONCLUSION

In conclusion, we have proposed a novel SIR algorithm by combining the HTETV regularization, which can be used for low-dose CT with combined noisy and sparse-view data acquisitions. Our approach has produced promising results in terms of preserving structural details and suppressing image noise. Furthermore, the proposed method can be extended to other topics in medical imaging, including interior reconstruction, metal artifact reduction, etc.

REFERENCES

[1] J. V. Spearman, U. J. Schoepf, M. Rottenkolber, et al, Effect of Automated Attenuation-based Tube Voltage Selection on Radiation Dose at CT: An Observational Study on a Global Scale[J]. *Radiology*. 279(1), 167-174 (2016).

[2] M. Li, C. Zhang, C. Peng, et al, Smoothed l_0 norm regularization for sparse-view X-ray CT reconstruction[J]. *BioMed Research International*. 2016(1), 1-12 (2016).

[3] Q. Xu, X. Mou, G. Wang, et al, Statistical Interior Tomography[J]. *Medical Imaging, IEEE Transactions on*. 30(5), 1116-1128 (2011).

[4] I. A. Elbakri and J. A. Fessler, Statistical image reconstruction for polyenergetic X-ray computed tomography[J]. *Medical Imaging, IEEE Transactions on*. 21(2), 89–99 (2002).

[5] E. A. Rashed and H. Kudo, Statistical image reconstruction from limited projection data with intensity priors[J]. *Physics in Medicine and Biology*. 57(7), 2039–2061 (2012).

[6] Zhang Y, Wang Y, Zhang W, et al, Statistical iterative reconstruction using adaptive fractional order regularization[J]. *Biomedical Optics Express*. 7(3), 1015-1029 (2016).

[7] C. Zhang, T. Zhang, M. Li, et al, Low-dose CT reconstruction via L1 dictionary learning regularization using iteratively reweighted least-squares[J]. *BioMedical Engineering OnLine*. 15(1), 1-21 (2016).

[8] E Y Sidky, Pan X C, Image Reconstruction in circular cone-beam computed tomography by constrained, total-variation minimization[J]. *Physics in Medicine and Biology*. 53(17), 4777-4807 (2008).

[9] Zhang X, Xing L, Sequentially reweighted TV minimization for CT metal artifact reduction[J]. *Medical Physics*. 40(7), 071907(1-12) (2013).

[10] Miao C, Yu H, A general-thresholding solution for l_p (0<p<1) regularized CT reconstruction[J]. *Image Processing, IEEE Transactions on*. 24(12), 5455-5468 (2015).

[11] H. Guo, J. Yu, X. He, et al, Improved sparse reconstruction for fluorescence molecular tomography with L1/2 regularization[J]. *Biomedical Optics Express*. 6(5), 1648-1664 (2015).

[12] M. M. Hyder, K. Mahata, An improved smoothed l_0 approximation algorithm for sparse representation[J]. *Signal Processing, IEEE Transactions on*. 58(4), 2194-2205 (2010).